Probabilistic Evaluation of Seismic Performance of Steel Moment Framed Buildings Incorporating Damper Limit States

H. Kit Miyamoto[1], Amir S.J. Gilani[2], Christopher Ariyaratana[3] and Akira Wada[4]

[1]CEO, Miyamoto International & Global Risk Miyamoto, 700 South Flower Street Suite 1010, Los Angeles, CA, 90017; PH (213) 362-7778;
Email: kmiyamoto@miyamotointernational.com
[2]Structural Specialist, Miyamoto International Structural and Earthquake Engineering, West Sacramento, CA., USA; Ph: (916) 373-1995;
Email: agilani@miyamotointernational.com
[3]Graduate Structural Engineer, Arup (Formerly University of Illinois), 499 Thornall Street - 9th Floor - Edison New Jersey 08837; PH (732) 623 7447
Email: chris.ariyaratana@arup.com
[4]Professor, Tokyo Institute of Technology, 4259 Nagatsuta-cho, Midori-ku, Yokohama, 226-8502, JAPAN; Email: awada@cv.titech.ac.jp

ABSTRACT

An advanced concept for design of steel moment framed structures, sizing steel members per code guidelines for strength and adding viscous dampers to limit story drifts, this results in robust structures with superior performance to that of conventional designs at the design and maximum considered earthquakes. However, the efficacy of such design at extreme events has not been well documented due to the lack of a comprehensive database detailing their responses and data on the structures with dampers subjected to very large earthquakes. The current research addresses the physical limit states of the dampers, and development of mathematical model of the viscous dampers incorporating such limit states. The adequacy of the model is then verified by correlating it with laboratory data. Next, nonlinear simulations of structures with viscous dampers are conducted to probabilistically determine the collapse performance of the buildings and draw conclusions about key factors affecting the response

INTRODUCTION

Viscous dampers were originally developed as shock absorbers for the defense and aerospace industries. In recent years, they have been used extensively for

seismic application for both new and retrofit building construction. During seismic events, the devices become active and the seismic input energy is used to heat the fluid and is thus dissipated. Subsequent to installation, the dampers require minimal maintenance. They have been shown to possess stable and dependable properties for design earthquakes. Figure 1 depicts the application of dampers to a new building in California (Miyamoto and Gilani, 2008).

To date, no comprehensive study has been undertaken to investigate the limit state of viscous dampers and to characterize the effect on the building once a damper limit state is reached. This paper presents some preliminary result from a comprehensive research currently underway to address this issue. Since dampers are ideal for drift control in steel moment frame buildings, the investigation is focused specifically on this type of construction.

MODELING OF VISCOUS DAMPERS

Component Of Viscous Dampers

Viscous dampers consist of a cylinder and a stainless steel piston. The cylinder is filled with an incompressible silicone fluid. The damper is activated by the flow of silicone fluid between chambers at opposite ends of the unit, through small orifices. Figure 2 shows the damper cross section.

Figure 1. Steel moment frame with dampers

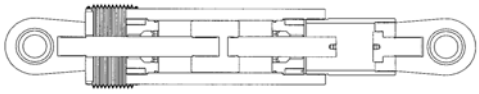

Figure 2. Viscous damper cross section

Simple Model

In most applications, the dampers are modeled as the simple model of Figure 3. The viscous damper itself is modeled as a dashpot in series with the elastic driver brace member. Such model is adequate for most design applications, but is not sufficiently refined for collapse evaluation. In particular, force and displacement limit states are unaccounted.

Damper Limit States

Although dampers are comprised of many parts, the limit states are governed by a few elements. These limit states include, but are not limited to, the stroke limit and force limit state. The stroke limit state is reached once the damper bottoms out, this occurs when the piston motion reaches its available stroke. Once this has occurred, the damper transitioned from a viscous damper to a steel brace with the stiffness equal to that of the cylinder wall. The force limit states in compression and tension are governed by the buckling capacity of the driver brace and the tensile capacity of the piston rod, respectively.

Advanced Model For Viscous Dampers

Figure 4 presents the proposed refined model for viscous dampers. This model

is developed to incorporate the limit states and consists of five components.

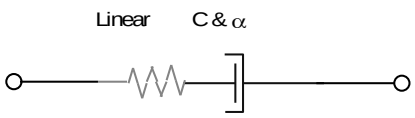

Figure 3. Simple model

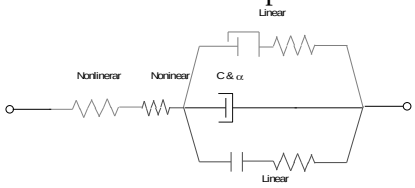

Figure 4. Advanced model

The damper components are as described in the following:

- The driver (KD), used to attach the damper to the beams and columns is modeled as a nonlinear spring.
- The piston rod (KP) and undercut is modeled as a nonlinear spring. The piston undercut is the machined down section between the end of the piston and the start of the piston male threaded part. In tension, the undercut section of the piston can yield and fracture.
- Dashpot (C and α) is used to model the viscous component.
- Gap element and linear springs (Kc) are used to model the limit state when the piston retraction equals the stroke (umax). The elastic stiffness depends on the damper construction and its cylinder properties.
- Hook elements and linear springs (Kc) are used to model the limit state when the piston extension reaches the damper stroke (umax). The stiffness is the same as that associated with the gap element.

Response Of The Limit State Model

In analysis, once a stroke limit is reached, the damper becomes numerically equivalent to a steel brace. Upon unloading, this process is reversed. When the force limit is reached, the entire damper is ineffective and thus permanently removed, even after unloading. The sudden transition between viscous damper, steel brace, and damper fracture can impart large impact forces on the structure.

At the instant that the gap closes, the damper force is zero. However, as loading is continued, the unit displacement can increase due to deformation in the cylinder wall and thus velocity is non-zero. At the large peaks, the damper force, which is the algebraic sum of the force in the dashpot and the cylinder wall, can be smaller than the force resisted by the wall cylinders. This is because the forces in the viscous element and cylinder wall can be out-of-phase.

ANALYTICAL SIMULATIONS

Overview

To illustrate the response of the refined model and illustrate its capability to capture all the limit states, analytical simulations were conducted. The damper was modeled in program OpenSEES (PEER 2009a) using the refined model. All analysis was conducted using a sinusoidal displacement loading function. The damper used in simulation was the 700-kN unit and has a constitutive relation (force in kN and velocity in mm/sec) of Eq. 1.

$$F = 88\,\mathrm{sgn}(v)|v|^{0.3} \tag{1}$$

Force Limit State Of Piston Fracture

This simulation was conducted to investigate the damper response for the limit state of piston undercut fracture. The stroke was artificially set to be large enough to

ensure that the damper did not bottom out in tension. The response is shown in Figure 5. Note that the force transmitted by the cylinder walls was zero since the damper had not bottomed out. Once the piston undercut reaches its tensile capacity, the damper element is automatically removed from the simulation and the forces drop to zero.

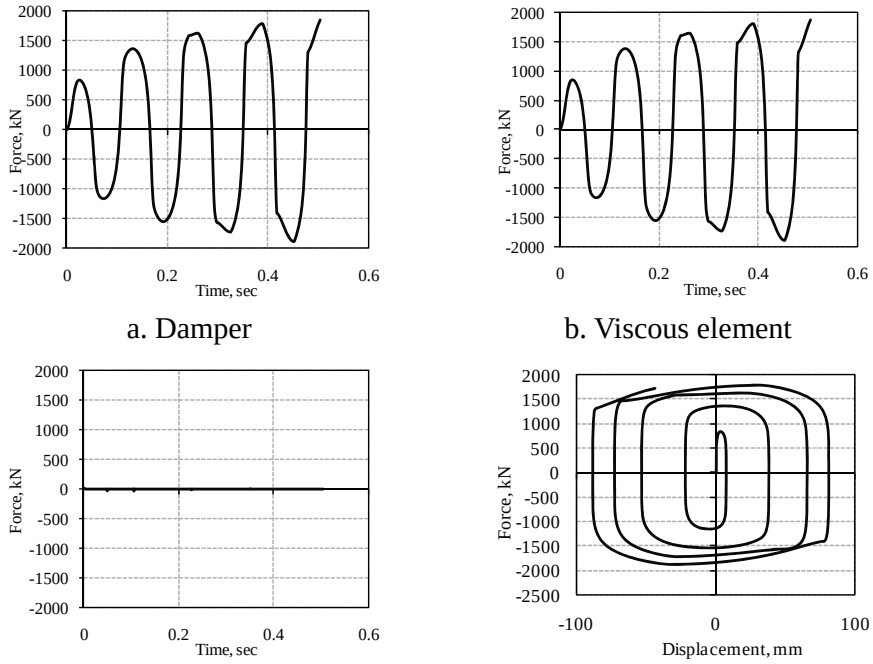

a. Damper b. Viscous element

c. Cylinder walls d. Damper hysteresis

Figure 5. Response when undercut fractures

Stroke Limit States

This simulation was conducted to investigate the damper response for the limit state when the stroke limit in extension and retraction are reached. The undercut tensile, piston and driver brace compressive capacity were artificially set to be large enough for these members to remain elastic. The response is shown in Figure 6. Note that the force transmitted by the cylinder walls is non-zero, once the stoke limit in either tension or compression was reached.

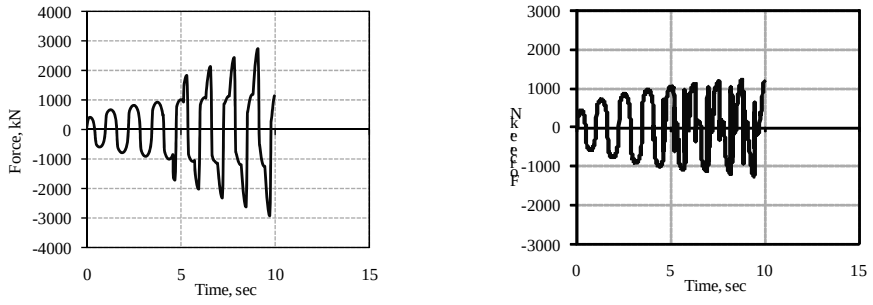

a. Damper b. Viscous element

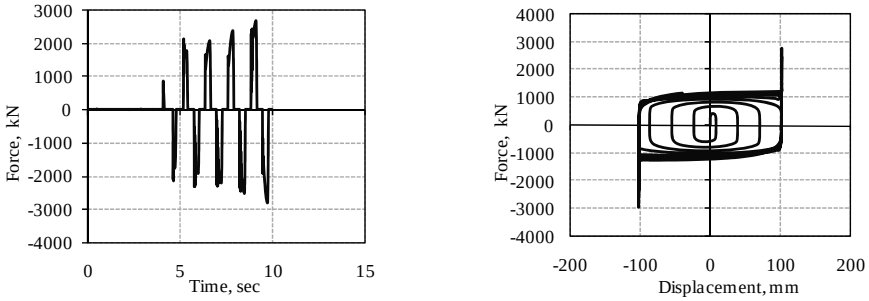

c. Cylinder walls d. Damper hysteresis

Figure 6. Response when damper bottoms out

Displacement And Force Limits

The stroke limit is reached first. If the loading was increased, then the driver would buckle in compression or the undercut would yield and fracture in tension. This simulation was conducted to investigate the damper response for the limit state of piston fracture following bottoming out of damper at full extension. The response is shown in Figure 7. At 4.5 sec in the response, the piston extension reaches the stroke limit and the damper bottoms out. At this point, velocity was zero and thus the force in the viscous element dropped to zero. The damper acted as an elastic brace. The undercut yielded but does not fracture. Loading is then reversed. This resulted in the disengagement of cylinder walls, and re-loading of the viscous component. At 5.3 sec, piston bottomed out again. The damper again became an elastic brace. Loading is increased further resulting in fracture of undercut. The entire damper was now ineffective and removed.

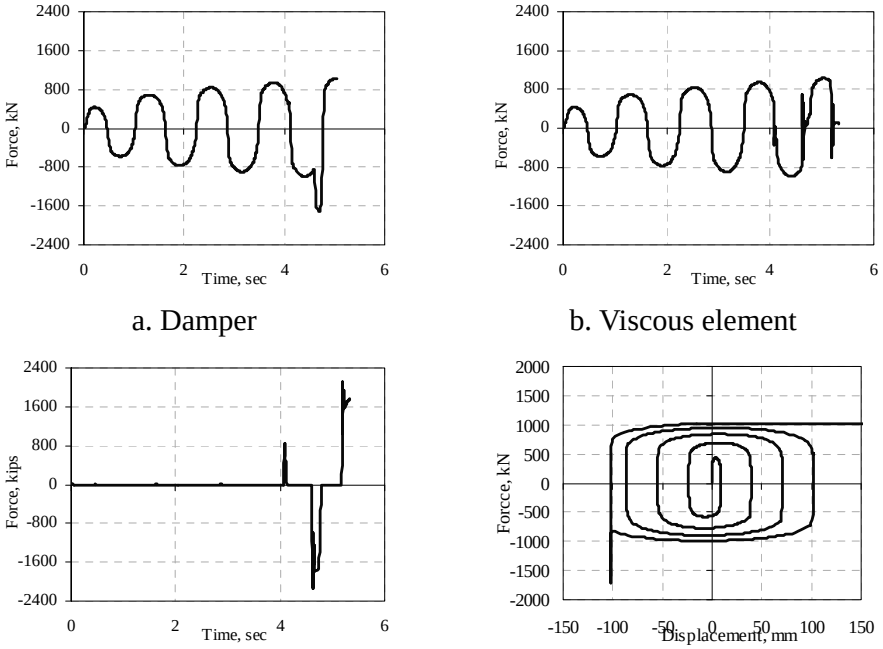

a. Damper b. Viscous element

c. Cylinder walls d. Damper hysteresis

Figure 7. Response for compound case

Correlation With Test Results

Experimental data from a damper (Taylor, 2009) was used to assess the accuracy of the refined mathematical model. This damper was laboratory tested and was subjected to large velocity and displacement pulses in succession and experienced several of its limit states. This damper had a nominal capacity of 2000 kN, a stroke of 140 mm, and constitutive relation (force in kN and velocity in mm/sec), of Eq 2.

$$F = 3.5\,\mathrm{sgn}(v)|v|^{0.5} \tag{2}$$

The damper was placed in the test rig and subject to a displacement loading history. The unit was placed with its piston extended to within 10 mm of the stroke limit prior to start of the displacement cycles.

The experimental displacement, velocity, and force responses are presented as solid lines in Figure 8a through Figure 8c, respectively. The displacement, velocity and force limit states are identified in these figures respectively.

At 4.30 sec, the unit was pulled in tension at 910 mm/sec and stopped just before it bottomed. This large velocity was close to 300% of its nominal design. This resulted in the forces developed in the damper that exceeded the nominal value computed from the constitutive relation.

At 4.61 sec, the damper bottomed out in tension, resulting in sharp increase in the measured force. This was followed by tensile yielding. The displacement response after this point was nearly flat with a slight increase due to yielding.

Finally at 4.68 sec, fracture occurs and the damper load drops to zero. After this time, no force can be transferred by the damper.

The dashed lines in these figures represent the results obtain from simulation using the refined damper element. Good correlation is obtained between the experimental data and analytical simulations. The analytical model was able to capture the bottoming of the damper and tensile fracture correctly.

Figure 8d presents the force-displacement hysteresis and the dissipated energy in the damper. The analytical model captures the experimental responses closely,

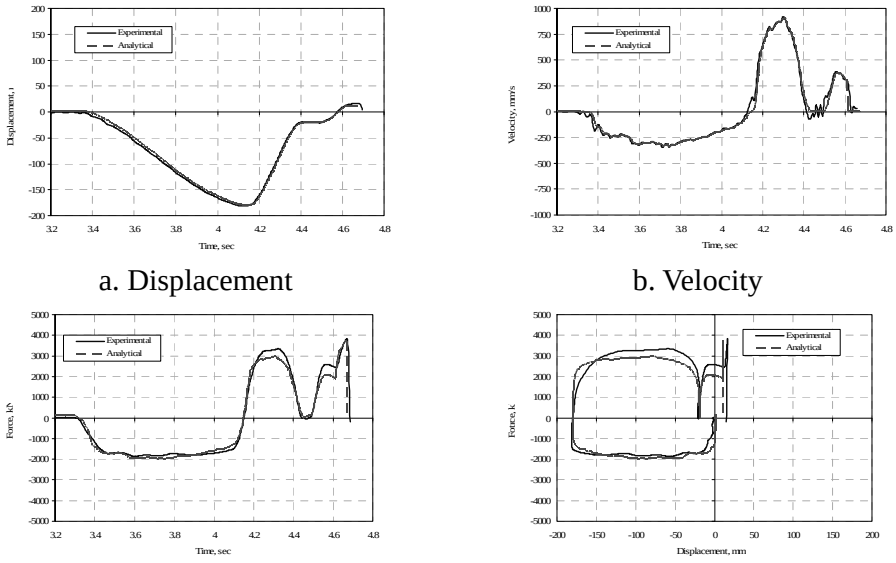

a. Displacement b. Velocity

c. Force d. Damper hysteresis

Figure 8. Experimental and analytical results

ANALYSIS PROCEDURE

Ground Motions

The input histories used in analysis were based on the two components of the 22 far-filed (measured 10 km or more from fault rupture) NGA PEER (2009b) records. These 44 records have been identified by FEMA P695 (FEMA 2009) for collapse evaluation analysis. The selected 22 records correspond to a relatively large sample of strong recorded motions that are consistent with the code (ASCE/SEI 7-05) (ASCE 2005) and are structure-type and site-hazard independent. Figure 9 presents the acceleration response spectra for these records. The design MCE spectrum is shown as the thick solid line in the figure. For analysis, the 44 records were first normalized and then scaled. Normalization of the records was done to remove the record-to-record variation in intensity.

Model Properties

Program OpenSees was used to conduct the nonlinear analyses described in this paper. Pertinent model properties are listed here.

- Analytical models were two-dimensional.
- Beam and column elements, were represented as one dimensional frame elements. The members were prismatic and linear.
- Material nonlinearity was represented by concentrated plastic hinges represented by RBS hinges placed at the center of the reduced section.
- The damper element was represented by the refined model including the limit states.

Incremental Dynamic Analysis (IDA)

For collapse analysis, the normalized records were then scaled upward or downward to obtain data points for the nonlinear incremental dynamic analysis (IDA) simulations (Vamvatsikos and Cornell, 2004).

APPLICATION TO STEEL BUILDINGS

General

To illustrate the concepts described in this paper, design and analysis of a single story structure with viscous damping was conducted. The one-story frame was square in plan and measures 27 m on each side. It is 4 m tall. The structure had one interior Special Moment Resisting Frame (SMRF) on the perimeter of each side. One of the 9x4 m frames was selected for design and analysis. Figure 10 presents the plan drawing for the structure. This design was representative of a typical office building built in Los Angeles California with the following conditions: Seismic Design Category D, S_S=1.5g and S_1 = 0.6g.

The frame was designed using the code provisions and special requirements for SMRFs. For this structure, the fundamental period (T1) was 0.42 sec. The ASCE/SEI 7 maximum period used to compute base shear (Tmax) was 0.31 second and was used for evaluation. Table 1 presents the properties of the archetypes.

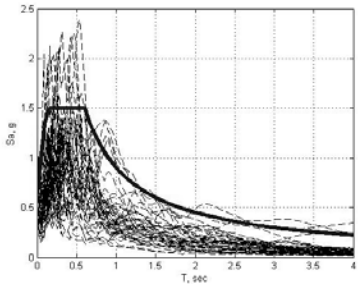

Figure 9.Response spectra of records

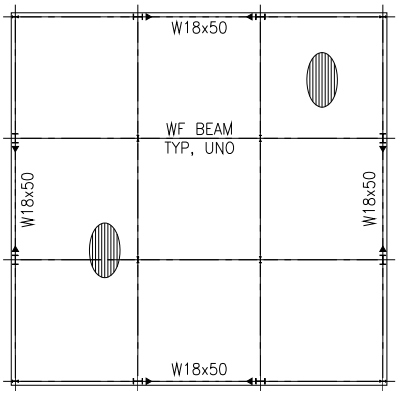

Figure 10. One story archetype

Table 1. Archetypes

Archetype	Stories	Column base	Story Drift Ratio, %	Damper FS
O1	1	Pinned	2.5%	1.0
O2	1	Pinned	1.0%	1.3
O3	1	Fixed	2.5%	1.0
O4	1	Fixed	1.0%	1.3

Pushover Results

Figure 11 presents the pushover curve for the archetypes O3 and O4. The solid and dashed lines correspond to the cases where dampers are excluded and included, respectively, in analysis. As long as the damper did not bottom out, the plots are identical. Once the damper bottomed out, there was significant increase in stiffness and strength since a stiff brace (cylinder wall) was now added to the system. After the damper failed, the damped pushover curve asymptotically approaches the undamped case. The dotted line corresponds to a bilinear approximation used to compute the yield and ultimate drifts and the corresponding ductility (μc). Using the building period and ductility, the spectral shape factor (SSF) is then computed. Note that O4 had a larger damper factor of safety and thus a larger increase in overall strength once the damper bottoms out. For all archetypes, the computed system ductility was 8.0 which resulted in a SSF of 1.34.

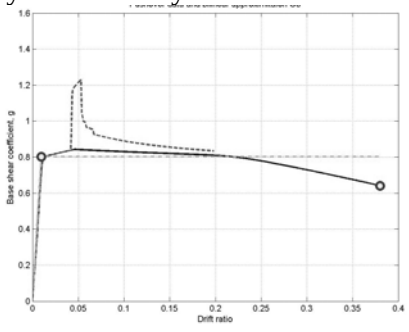

a.O3

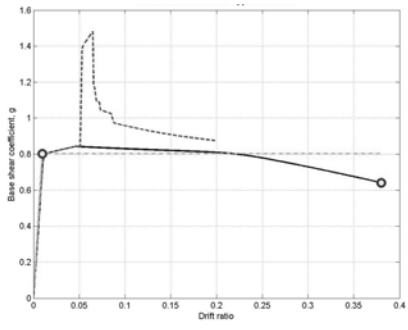

b.O4

Figure 11. Static pushover curves

IDA results

Figure 12 presents the IDA plots for the O1and O2. frame. The solid and dashed red lines correspond to the MCE (SMT) and the median collapse capacity (SCT), respectively. Note that the addition of small damper factor of safety

significantly increased collapse margin. The collapse margin ratio (CMR) is defined as the ratio of SCT and SMT. The adjusted collapse margin ratio (ACMR) is then computed as the product of SSF and CMR. FEMA P695 specifies a minimum ACMR of 1.59 for acceptable performance. As shown in Table 2, all archetypes have significantly larger collapse margins and therefore pass easily.

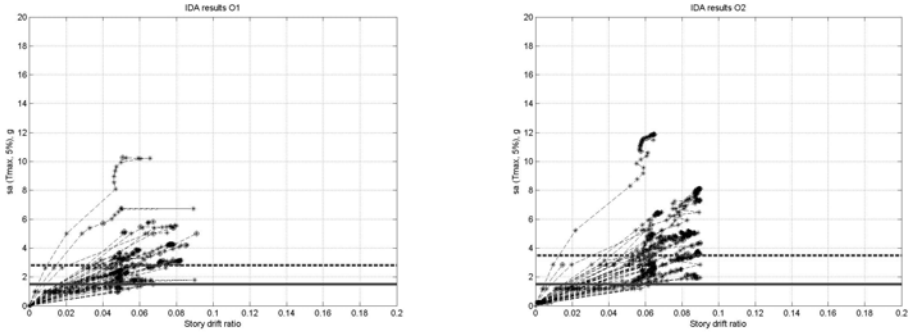

a. O1 b. O2

Figure 12. IDA plots

Table 2. Collapse margins for archetypes.

Archetype	SCT	SMT	CMR	SSF	ACMR	P/F
O1	2.79	1.50	1.86	1.34	2.49	Pass
O2	3.49	1.50	2.33	1.34	3.12	Pass
O3	5.27	1.50	3.51	1.34	4.71	Pass
O4	6.12	1.50	4.08	1.34	5.47	Pass

Fragility Data

Figure 13 presents the fragility plots for O1 and O2. The 44 collapse data are statistically organized (data points in the figures) and a lognormal curve was fitted to the data (dashed lines in the figures). The plot was then rotated to correspond to a total uncertainty of 0.55 (solid line) per FEMA P695. Finally the curve was shifted to account for the effect of the SSF (dark solid lines in the figures). The probability of collapse at MCE intensity was then computed using the fragility curves as listed in Table 3. Note that the probability of collapse at MCE level was reduced by a factor of approximately 2.5 when an additional damper factor of safety of 30% is included in design. Such small increase is cost efficient and provides significant additional protection to the structure.

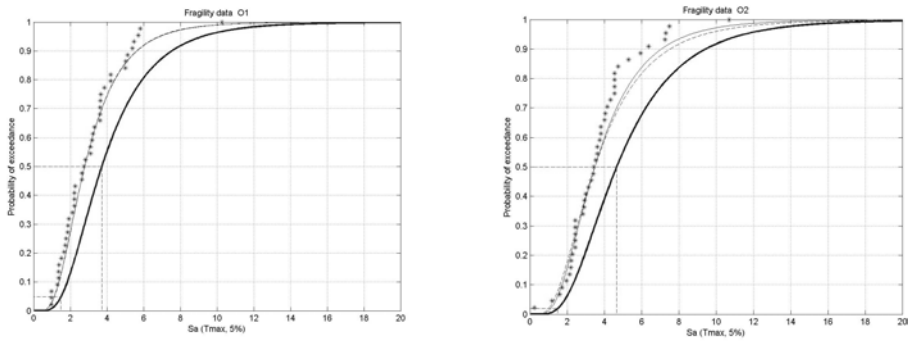

a. O1 b. O2

Figure 13. Fragility plots

Table 3. Collapse probability for archetypes at MCE.

Archetype	MCE Probability of collapse %
O1	4.9
O2	2.0
O3	2.5
O4	1.0

Damper Responses

Figure 14 and Figure 15 presents the fragility plots for the damper stroke and force, respectively. For each response quantity and archetype, the 44 data points for the damper reaching its stroke or force limit states were statistically organized (data points in the figures) and a lognormal curve is fitted to the data (dashed lines in the figures). The plot was then rotated to correspond to a total uncertainty of 0.55 per FEMA P695 (solid line). The probability of the damper reaching its limit state at the MCE intensity can then be computed from the fragility plots. At MCE intensity the probability of collapse can then be computed using the fragility curves as listed in Figure 14. Note that the probability of damper reaching a limit state is significantly reduced when a damper factor of safety of 30% is included in design. Such small increase is cost efficient and provides significant additional protection to the dampers.

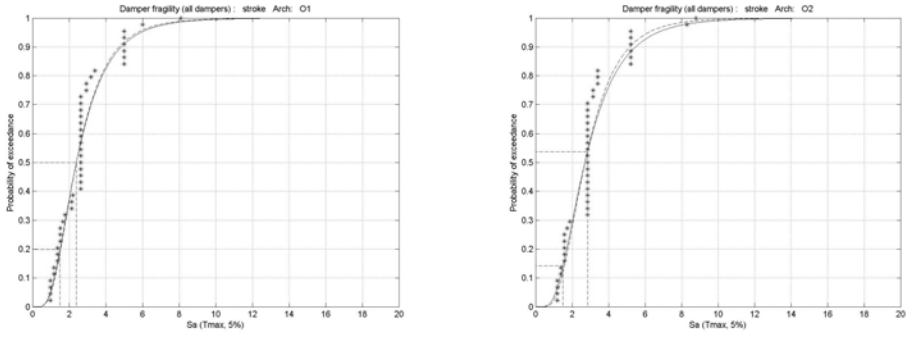

a. O1 b. O2

Figure 14. Damper stroke fragility

Table 4. Damper fragility data.

Archetype	Median Sa intensity to reach limit		Probability of reaching limit state at MCE	
	Stroke	Force	Stroke	Force
O1	2.39	2.95	20%	11%
O2	2.71	3.60	14%	6%
O3	3.83	5.89	6%	0.6%
O4	3.84	6.11	4%	0.5%

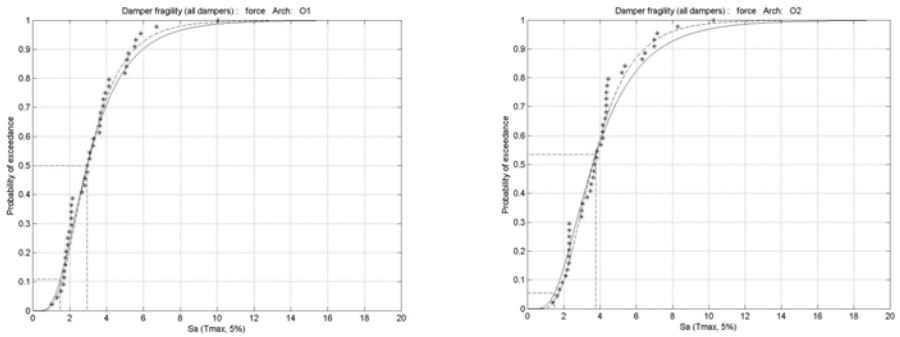

a. O1 b. O2

Figure 15. Damper force fragility

ONGOING RESEARCH

The ongoing research at the Tokyo Institute of Technology by the authors is intended to expand the knowledge base for steel SMRF buildings with dampers. The research closely follows the guidelines and procedures established by ATC 63 (NEHRP 2009).

A total of 15 archetypes (from one to thirty story buildings) are currently under consideration. The basic geometry and distribution of dampers for these models are summarized in Table 5. The selected building models are regular in plan and elevation with a dominant first mode response. The period of tall buildings is limited to approximately 5 sec to ensure sufficient energy is present in the input histories.

Table 5. **Archetypes.**

Archetype	Stories	Column base	Story Drift Ratio, %	Damper FS
O1	1	Pinned	2.5%	1.0
O2	1	Pinned	1.0%	1.3
O3	1	Fixed	2.5%	1.0
O4	1	Fixed	1.0%	1.3
A1	2	Pinned	2.5%	1.0
A2	2	Pinned	1.0%	1.3
A3	2	Fixed	2.5%	1.0
A4	2	Fixed	1.0%	1.3
B1	5	Fixed	2.0%	1.0
B2	5	Fixed	1.0%	1.3
C1	10	Fixed	2.0%	1.0
C2	10	Fixed	1.0%	1.3
D1	20	Fixed	2.0%	1.0
D2	20	Fixed	1.0%	1.3
E1	30	Fixed	1.0%	1.0

CONCLUSIONS

New steel buildings were designed using performance based engineering and the provisions of ASCE/SEI 7. Special Moment Resisting Frames were used to provide strength; dampers were used to control story drifts. This design

methodology proved to be superior compared to conventional. The demand on both structural and non-structural components was reduced.

To date, a model of viscous dampers with limit states has been formulated that includes damper limit states.

Current research using Incremental Dynamic Analysis and limit states of dampers is currently underway. The outcome of this study will provide a more realistic assessment of the performance of moment frames with dampers.

All the archetypes had significant margin against collapse and thus had satisfactory performance. When an additional damper factor of safety is included in design, additional protection for the structures and dampers is provided.

As one of the research deliverables, pertinent information will be provided for the designers to assist in seismic design using this viscous dampers

ACKNOWLEDGEMENTS

This work was supported in large part by Taylor Devices, Inc and Armour Steel. The authors acknowledge their financial support. The technical assistance of Mr. Doug Taylor and Mr. John Metzger of Taylor Devices is acknowledged. Professor Curt Haselton of the California State University, Chico provided guidance for this study.

REFERENCES

American Society of Civil Engineers (ASCE) (2005). "*ASCE 7-05: Minimum Design Load For Buildings And Other Structures*," American Society of Civil Engineers, Reston VA.

Miyamoto, H.K., and Gilani, A.SJ. (2008). "Design of a new steel-framed building using ASCE 7 damper provisions," *Proceedings of ASCE SEI institute. Structures Congress*,

National Earthquake Hazards Reduction Program (NEHRP) (2009). *ATC 63, FEMA P695: Quantification of Building Seismic Performance Factors*, Federal Emergency Management Agency, Washington D.C.

Pacific Earthquake Engineering Research Center (PEER) (2009a). Open System for Earthquake Engineering Simulation (OpenSees), McKenna, F., Fenves, G., et al, Pacific Earthquake Engineering Research Center, University of California, Berkeley, Berkeley CA.

Pacific Earthquake Engineering Research Center (PEER) (2009b). *PEER Next Generation Attenuation (NGA) Records*, Pacific Earthquake Engineering Research Center, University of California, Berkeley. Berkeley CA.

Taylor Devices (2009). Personal Communications.

Vamvatsikos, D. and Cornell, A.C. (2004). "Applied Incremental Dynamic Analysis", *Earthquake Spectra*, Earthquake Engineering Research Institute Oakland, CA. **20(2),** 523–553.